Targeted alpha immunotherapy of CD20-positive B-cell lymphoma model: Dosimetry estimate of 225Ac-DOTA-rituximab using 64Cu-DOTA-rituximab

Chul-Hee Lee
  Korea Institute of Radiological and Medical Sciences

Ilhan Lim
  Korea Institute of Radiological and Medical Sciences

Sang-Keun Woo
  Korea Institute of Radiological and Medical Sciences

Wook Kim
  Korea Institute of Radiological and Medical Sciences

Kwang Il Kim
  Korea Institute of Radiological and Medical Sciences

Kyo Chul Lee
  Korea Institute of Radiological and Medical Sciences

Kanghyon Song
  Korea Institute of Radiological and Medical Sciences

Sang Moo Lim
  Korea Institute of Radiological and Medical Sciences

Original research

Keywords: CD20-positive B-cell lymphoma, rituximab, 64Cu, PET, Monte Carlo simulation, 225Ac

---

Abstract

Purpose: To evaluate the radiation dosimetry of 225 Ac-DOTA-rituximab using Monte Carlo simulation of 64 Cu-DOTA-rituximab.

Methods: CD20 expression was evaluated in lymphoma cell lines (Jurkat and Raji). DOTA-rituximab was conjugated and then chelated by 64 Cu. Tumor xenograft models were established in BALB/c-nu mice. Animal PET/CT imaging was obtained after tail vein injection with and without a pre-dose of 2 mg of cold rituximab. Specific binding of tumors was evaluated by an organ distribution assay and autoradiography. CD20 expression in tumor tissues was evaluated by immunohistochemistry. The residence time was calculated using 64 Cu-DOTA-rituximab PET/CT acquisition data using OLINDA/EXM software. 225 Ac-DOTA-rituximab dosimetry analysis was performed using Monte Carlo simulation.

Results: CD20 protein was highly expressed in Raji cells. Specific binding of Raji cells was 90 times that of Jurkat cells (p<0.0001). Immunoreactivity was more than 75%. PET/CT imaging with 64 Cu-DOTA-rituximab was specifically observed in tumors. The radioactivity of the tumor was much higher than that of other organs, and tumor uptake was related to CD20 expression. The predicted human dose for the administration of 64 Cu-DOTA-rituximab was measured as the effective dose (3.20E-02 mSv/MBq). In the tumor region, equivalent doses of 225 Ac-DOTA-rituximab (14 Sv RBE5 /MBq) were much higher (74-fold) than those of 64 Cu-DOTA-rituximab (0.19 Sv RBE5 /MBq) (p<0.01).

Conclusion: Tumor dosimetry of 225 Ac-DOTA-rituximab can be estimated via the Monte Carlo simulation of 64 Cu-DOTA-rituximab. 225 Ac-DOTA-rituximab can be used as targeted alpha therapy for patients with refractory lymphoma.

Introduction

Radioimmunotherapy (RIT) using beta-emitters such as ^{90}Y or ^{131}I has become an innovative method for B-cell non-Hodgkin's lymphoma (NHL) treatment [1–3]. Among these radiopharmaceuticals, ^{131}I-rituximab plays a role in treating patients with aggressive CD20-expressing B-cell NHL [4–7]. Our institute has used RIT for NHL patients using ^{131}I-rituximab [8–12]. RIT using ^{131}I-rituximab showed remarkable treatment results, but some patients experienced recurrence after RIT, which reveals resistance to the treatment. In this situation, more effective treatment modalities are required for better clinical outcomes.

Recently, targeted alpha therapy (TAT) was attempted and exhibited excellent results in certain diseases. TAT has been found to overcome resistance to beta emitters because the linear energy transfer (LET) of beta-emitters is low (0.1–1.0 keV/μm), while that of alpha-emitters (50–230 keV/μm) is high [13]. In this regard, it is a good strategy to apply rituximab RIT with alpha-emitter radionuclides such as Actinum-225 (^{225}Ac).

Ac-225 decays into ^{221}Fr, and finally to the more stable ^{209}Bi, yielding the four alpha-emitters [14]. Some studies using the PSMA inhibitor, PSMA-617, demonstrated that ^{225}Ac-PSMA-617 contributes to the

dramatic benefit in metastatic castration-resistant prostate cancer patients [15, 16]. Other studies utilising antibodies also showed the effectiveness and safety of TAT [17–19]. Accordingly, [225]Ac is a potent candidate for the radionuclide of RIT because its half-life of [225]Ac is 9.92 days [20] and rituximab has been known as an antibody with a long half-life, which is 2–7 days [21].

However, no study has evaluated [225]Ac-DOTA-rituximab in CD20-positive human B-cell lymphoma. In this study, we estimated the feasibility of RIT with [225]Ac-DOTA-rituximab in a CD20-positive B-cell lymphoma model through Monte Carlo simulation using ^{64}Cu-DOTA-rituximab. To perform this, we established a CD20-positive human lymphoma xenograft model to evaluate targeted imaging for non-invasive *in vivo* monitoring of lymphoma using ^{64}Cu-DOTA-rituximab PET and evaluated the correlation between CD20 expression and specific binding of ^{64}Cu-DOTA-rituximab in tumour tissue. For further human patient studies, we estimated dosimetry using biodistribution results and quantitative analysis of ^{64}Cu-DOTA-rituximab PET imaging.

Materials And Methods

Antibody and Cell lines

CD20 targeted rituximab (Mabthera) was purchased from Roche. Human lymphoma cell lines (Jurkat and Raji) were used. Both cells were obtained from American Type Culture Collection (ATCC) and maintained in RPMI 1640 with 10% fetal bovine serum (Gibco) containing 1% antibiotics (penicillin G, 100 unitsmL, and streptomycin 10 µgml; Gibco). Cells were incubated at 37 °C in a 5% CO_2 atmosphere.

Western blot

Protein concentrations were determined using a BCA protein assay kit (Thermo Scientific). The membranes were blocked for 1 hour at room temperature and incubated with either anti-CD20 (#sc-58985) or β-actin (#A5441, Sigma-Aldrich) primary antibodies overnight at 4 °C. An enhanced chemical luminescence reagent (Roche) was used, and luminescent signals were measured with a ChemiDoc imaging system (Bio-Rad).

Immunoconjugation of DOTA-rituximab

For the desalting process of rituximab, we exchanged non-metallic D. W (D. W) using Amicon® ultra centrifugal filters (Millipore). The DOTA (1,4,7,10-tetraazacyclododecane-1,4,7,10tetraacetic acid)-NHS ester was purchased from FutureChem (#FC-2134, Seoul, Korea). Briefly, 10 mg rituximab was added to 200 µL of 1 M sodium bicarbonate (pH 8.0) for 5 min. DOTA-NHS (7 nM) was added to the mixture at 4 °C overnight. Excess DOTA-NHS ester was removed using a PD-10 column (GE Healthcare) using 1 mM sodium acetate buffer (pH 5.5). The number of chelators per antibody was calculated by matrix-assisted laser desorption ionisation time-of-flight mass spectrometry (MALDI-TOF MS) to compare the molecular weights of DOTA-rituximab and rituximab.

Radiolabelling and Stability Tests

^{64}CuCl2 was produced at the Korea Institute of Radiological and Medical Sciences (Seoul, Korea) by 50 MeV cyclotron irradiation [22]. The ratio of ^{64}CuCl$_2$ activity per DOTA-rituximab was determined to be 2 MBq per 1 mg. DOTA-rituximab conjugate was incubated with dried ^{64}CuCl2 in 1 mM sodium acetate buffer at 40 °C for 30 min. The radiolabelling yield was evaluated by instant thin-layer chromatography (iTLC) without additional purification. The stability of ^{64}Cu-DOTA-rituximab was analysed through iTLC after incubation in human and mouse serum, and phosphate buffered saline (PBS) at 37 °C for various times (1, 2, 6, 24, 48, and 60 h).

Cell binding assays and immunoreactivity

Cell binding with ^{64}Cu-DOTA-rituximab was performed using Jurkat and Raji cells. Both, Jurkat and Raji cell set-ups (5×10^5 cells /500 μL in tube) were incubated for 3 h in triplicate. Nonspecific binding (competitive inhibition) was performed by adding 11 μM of cold rituximab. After incubation, the cells were rinsed twice with cold PBS containing 1% bovine serum albumin (BSA). Cell bound radioactivity (count per minute) was evaluated using a γ-counter (Wizard 1480, Perkin-Elmer). Specific binding (%) was calculated using total binding and nonspecific binding data. To evaluate immunoreactivity [23], 3.1 nM of ^{64}Cu-DOTA-rituximab was added to Raji cells diluted from 1×10^7 cells/tube to 0.016×10^7 cells/tube in 500 μL serum-free medium. The incubation time, washing, and calculation methods were the same as above. The immunoreactive fraction was determined by performing a linear regression analysis of the double inverse plot of total/bound activity versus normalised cell concentration. The immunoreactive fraction was then obtained from the inverse of the intercept on the plot. Data analysis was performed using GraphPad Prism software.

Animal experiments

Six-week-old female BALB/c-nude mice were obtained from NARA Bio, Inc. All animal experiments were approved by the Institutional Animal Care and Use Committee of KIRAMS (2018-0061). For establishment of lymphoma xenograft mouse models (*n=5;* for PET/CT imaging, *n=3;* for biodistribution), Raji cells (5×10^7/ in 200 μL PBS) were transplanted subcutaneously into the right thigh. Small animal PET imaging and biodistribution studies were performed when tumour sizes were > 0.5 cm in diameter.

Small-animal PET/CT imaging

PET/CT images of tumour-bearing mice were acquired using PET/CT (INVEON scanner, Siemens Healthcare). Images were obtained for 20 min under inhalation anaesthesia (isoflurane, 1.5%) at 2, 24, and 48 h after intravenous injection (*i.v.*) of 7.4 − 7.7 MBq of ^{64}Cu-DOTA-rituximab per mouse. Blocking studies (*n=2*) were evaluated for CD20 specificity of ^{64}Cu-DOTA-rituximab. Non-labelled rituximab (10 mgmL) was injected intravenously within 2 h before ^{64}Cu-DOTA-rituximab injection. Images were reconstructed with INVEON software and the AMIDE algorithm (A Medical Image Data Examiner).

Biodistribution study

Biodistribution studies were performed to evaluate the uptake of ^{64}Cu-DOTA-rituximab in tumour-bearing mice or normal mice. All mice were intravenously injected with 1.85 MBq of ^{64}Cu-DOTA-rituximab. Tumour-bearing mice (*n=3*) were sacrificed 48 h after *i.v.* injection. For dosimetry, normal mice (*n=4*/group) were sacrificed at 1, 2, 6, 24, 48, and 72 h after *i.v.* injection. Various organs containing tumours and blood samples were weighed, and the radioactivity was measured. The γ-counter data were represented by the percentage of injected dose per gram of tissue (%ID/g).

Autoradiography and Immunofluorescence

After the γ-counting of tumours from the biodistribution study, tumour tissues were frozen using optimal cutting temperature (OCT) compound at -80 °C. A cryostat microtome (CM1800, Leica Instruments) was used for frozen sections of tumours tissue (15 μm depth in non-coating slide). The frozen sections were exposed on a film for 7 days in a deep freezer, and the film was scanned with BAS-5000 (Fujifilm). The image intensity of photostimulated luminescence was analysed using Fujifilm Multi Gauge software, version 3.0 (Fujifilm).

For immunostaining, a cryostat microtome was used for frozen sections of the tumours (7 μm depth in coating slide). Briefly, the slides were rinsed using PBS for 10 min and fixed in 4% paraformaldehyde for 10 min. After being washed twice, the slides were incubated in Triton X-100 for 10 min to permeate the tumours tissue. Normal goat serum (1%) was used for non-specific binding and incubated with anti-CD20 (#sc-58985) primary antibody overnight at 4 °C. To visualise specific binding of the antibody, fluorescence-labelled secondary anti-mouse antibody (Bethyl lab) was added to the slides for 1 h. Immunofluorescence images were obtained using IN Cell Analyzer 2200 (GE Healthcare).

Dosimetry calculation

Residence time and human extrapolation dosimetry analysis were performed using the OLINDA/EXM software (Organ-Level Internal Dose Assessment/Exponential Modeling computer software, Vanderbilt University, 2003). The residence time was calculated at each time point for 2, 24, 48 h ^{64}Cu-DOTA-rituximab PET/CT acquisition data. The calculated region-of-interest (ROI) was defined based on the CT image. The ^{225}Ac-DOTA-rituximab dosimetry analysis was performed using Monte Carlo simulation. The absorbed dose of ^{225}Ac-DOTA-rituximab also considered all daughter radionuclides (^{221}Fr, ^{217}At, ^{213}Bi, ^{213}Po, ^{209}Tl, and ^{209}Pb) and summed up after applying weighting factors in the two possible pathways, 2% for ^{209}Tl and 98% for ^{213}Po.

S-value and Absorbed dose calculation

The S-value was acquired from tumours and organ tissue density. CT density and PET radioactivity information were used as input data. The S-value and dose map of the tumours and organs were calculated using Geant4 Monte Carlo simulation. The S-value equation is as follows:

$$S(r_{target} \leftarrow r_{source}) = \frac{k \sum y_i \, E_i \emptyset_i (r_{target} \leftarrow r_{source})}{m_{target}}$$

where y_i is the number of energy, E_i is the energy per radiation, and m is the mass of the target region.

The absorbed dose (Dr_T) was calculated using the following formula:

$$D_{r_T} = A_0 \sum_i \tilde{A}_{r_j} \cdot S(r_T \leftarrow r_s)$$

where A_0 is the initial injected radioactivity and $\tilde{A}_{r_j}$ is the radiotracer residence time of a source organ r_j. $S(r_T \leftarrow r_s)$ is the dose deposited in the target r_T per unit of cumulated activity in source r_s. The absorbed dose of each organ and tumours was calculated for each organ, including contributions from the self-dose with the cross-dose from other segmented regions [24].

Statistical analysis

All statistical analyses were performed using GraphPad Prism software. All data are evaluated as means ± standard deviation (SD) and are representative of at least two separate biological experiments performed in triplicate. Statistical significance between groups was compared using one-way ANOVA and unpaired Student's t-test. P < 0.05 was considered statistically significant.

Results

Specific CD20 targeting of ^{64}Cu-DOTA-rituximab

The mass difference between DOTA-rituximab and rituximab was about 1093 (m/z), and consequently we confirmed that the number of DOTA chelates per rituximab was approximately 2.8±0.21 (Supplementary Table 1). The radiolabeling efficiency was over 95% (Supplementary fig. 1a), and the stability of ^{64}Cu-DOTA-rituximab was over 90% in human and mouse serum, and in PBS (Supplementary fig. 1b). CD20 expression was observed only in Raji cells (Fig. 1a). Specific binding of ^{64}Cu-DOTA-rituximab in Raji cells was 90-fold higher than that in Jurkat cells *(p<0.0001)*. Between non-specific binding and total binding in Raji cells, the binding effect of ^{64}Cu-DOTA-rituximab was found to be significantly higher in total binding in Raji cells, by as much as 95-fold *(p<0.01)* (Fig. 1b). Immunoreactivity was observed at 76%, which was similar to that observed in a study by Natarajan et al. [25] (Fig. 1c and 1d).

^{64}Cu-DOTA-rituximab PET/CT imaging in lymphoma models

To evaluate the *in vivo* PET imaging of lymphoma using ^{64}Cu-DOTA-rituximab, we established CD20-positive lymphoma xenograft models using Raji cells. We expected that these mouse models would

reflect the distribution of ^{64}Cu-DOTA-rituximab in lymphoma patients. Confirmation of the formation of the lymphoma model was done using ^{18}F-FDG. Localized FDG uptake was observed at the xenograft site of the lymphoma model **(Supplementary fig. 2)**. In the ^{64}Cu-DOTA-rituximab PET study, focal FDG uptake was found in CD20 positive tumours at 24 h and 48 h (not shown at 2 h), but there was less uptake in the cold rituximab pre-injection group **(Fig. 2a)**. These uptake differences were remarkable at 48 h maximum intensity projection image from ^{64}Cu-DOTA-rituximab PET/CT **(Fig. 2b)**. In biodistribution results at 48 h, the distribution of ^{64}Cu-DOTA-rituximab in tumortumour groups revealed similar results, compared to the normal mice group without xenograft **(Fig. 2c)**. Autoradiography of the extracted tumortumour indicated a high correlation between autoradiography and immunohistochemistry with CD20 positive areas of the tumortumour **(Fig. 2d)**. Consequently, we demonstrated that ^{64}Cu-DOTA-rituximab specifically targeted CD20 positive tumorstumours.

Equivalent dose calculation of ^{225}Ac-DOTA-rituximab using ^{64}Cu-DOTA-rituximab

To estimate the therapeutic effect of ^{225}Ac-DOTA-rituximab for targeted alpha-therapy using ^{64}Cu-DOTA-rituximab, S values were calculated with both ^{64}Cu [26] and ^{225}Ac (data not shown) by means of Monte Carlo simulation with the CT images. The equivalent dose (Sv_{RBE5}/MBq) of ^{64}Cu-/^{225}Ac-DOTA-rituximab in the heart, lung, liver, kidney, spleen, and tumour region was calculated. In the ^{64}Cu-DOTA-rituximab group, the highest equivalent dose was found in the tumour (0.19 Sv_{RBE5}/MBq), followed by the heart (0.14 Sv_{RBE5}/MBq) and lung (0.12 Sv_{RBE5}/MBq) **(Fig. 3a)**. On the other hand, the heart (34 Sv_{RBE5}/MBq) had the highest equivalent dose in the ^{225}Ac- DOTA-rituximab group **(Fig. 3b)**. With regards to the tumour equivalent dose, ^{225}Ac-DOTA-rituximab dose (14 Sv_{RBE5}/MBq) was 74 times the ^{64}Cu-DOTA-rituximab (0.19 Sv_{RBE5}/MBq) dose **(Fig. 3c3M)** (*p<0.01*).

Discussion

The current study aimed to evaluate radiation dosimetry for ^{225}Ac-DOTA-rituximab in CD20-positive B-cell lymphoma xenograft models. We demonstrated that ^{64}Cu-DOTA-rituximab specifically targeted CD20-positive lymphoma xenograft in terms of cell binding assay, biodistribution, autoradiography, and tissue staining as well as *in vivo* PET/CT imaging. In addition, we calculated the equivalent dose for ^{225}Ac-DOTA-rituximab TAT using Monte Carlo simulation of ^{64}Cu-DOTA-rituximab PET imaging.

The results of the present study correspond with those of a previous study, in which the biodistribution of ^{227}Th-DOTA-rituximab was similar to that of ^{64}Cu-DOTA-rituximab [27–29]. However, the equivalent dose of ^{227}Th-DOTA-rituximab (50 Sv_{RBE5}/MBq) [27] was lower than those of ^{64}Cu-DOTA-rituximab (0.19 Sv_{RBE5}/MBq), and ^{225}Ac -DOTA-rituximab (14 Sv_{RBE5}/MBq) because they are different radionuclides. Furthermore, these values were calculated using different methodologies. We maintain that this study's equivalent dose is more accurate than the radiation dose of ^{227}Th-DOTA-rituximab because the absorbed

dose was estimated using the area under the curve of the time activity curve, [27] while this study analysed the equivalent dose using the tumour S value of the Monte Carlo simulation.

[64]Cu-DOTA-rituximab was previously reported by Natarajan et al. as a radiopharmaceutical agent for diagnostic PET imaging [25]. This result was first presented from synthesis to dosimetry for human patients using a transgenic mouse model expressing huCD20 in the kidney. However, mouse xenograft models bearing human lymphoma cells were not studied using ^{64}Cu-DOTA-rituximab. Therefore, to obtain a tumour-targeting effect with organ distribution pattern of ^{64}Cu-DOTA-rituximab, we developed a CD20-positive lymphoma xenograft model. In our study, ^{64}Cu-DOTA-rituximab was also specifically bound to only CD20 positive lymphoma cells (Fig. 1). Furthermore, specific uptake in tumour was observed through PET/CT imaging, and the distribution pattern of ^{64}Cu-DOTA-rituximab in tumour models was evaluated (Fig. 2). Additionally, we confirmed biodistribution and residence time in normal mice (**Supplementary Fig. 3**). In a normal biodistribution study, the half-life of ^{64}Cu-DOTA-rituximab in mouse blood was estimated to be approximately 6–21 h [30]. Consequently, these results suggest that ^{64}Cu-DOTA-rituximab specifically targets CD20-positive human B-cell lymphoma.

Generally, the pharmacokinetics of therapeutic radiopharmaceuticals are analysed using diagnostic radionuclides. For example, some studies prefer to use [124]I-mIBG PET/CT images for ^{131}I-mIBG targeted radionuclide therapy as a means for better treatment planning [31]. In addition, the radiation dosimetry of [213]Bi-PSMA-617 was estimated using ^{68}Ga-PSMA-617 imaging in patients for clinical application of alpha radionuclide therapy [32]. As a positron emitter, ^{64}Cu is also an attractive diagnostic radionuclide for PET imaging [33]. Using ^{64}Cu, Woo et al. calculated the absorbed dose of [67]Cu-DOTA/NOTA-trastuzumab to evaluate the therapeutic effect of HER2-positive breast cancer [26]. Based on this method, we estimated the radiation dosimetry of [225]Ac-DOTA-rituximab using ^{64}Cu-DOTA-rituximab PET/CT imaging from CD20-positive human B-cell lymphoma models (Fig. 3). The OLINDA/EXM software is widely used for the analysis of normal organ dosimetry. However, this software has been used for human digitalised phantoms, and its limitation is that it cannot calculate abnormal regions such as the tumour region. For this reason, we performed a Monte Carlo simulation to calculate the absorbed dose in the tumour regions. Our results demonstrated that [225]Ac-DOTA-rituximab showed a significantly larger equivalent dose than ^{64}Cu-DOTA-rituximab (Fig. 3c). Consequently, a low dose of [225]Ac-DOTA-rituximab can be applied to provide targeted therapy by releasing high LET alpha-emitters.

High LET alpha particles are promising candidates for killing target cells. Among them, [225]Ac plays an important role in targeted alpha therapy (TAT) and can be used efficiently and safely [34]. Some studies have shown that high energy within a short range induces DNA damage at least 100-fold higher than beta particles [35], and DNA double strand breakage (DSB) has therapeutic effects [36]. With regard to radiation dose, another study revealed that the radiation dose (Gy/Bq) of [225]Ac was 900 times that of lutetium-177 (^{177}Lu) and 14 times that of radium-223 ([223]Ra) through Monte Carlo simulation [37]. This result could explain why equivalent doses of [225]Ac-DOTA-rituximab in major organs were higher than

those of ^{64}Cu-DOTA-rituximab and tumour (Fig. 3a **and b**). Similarly, TAT using ^{225}Ac-DOTATOC triggers much higher γH2AX-foci formation from DSB than ^{177}Lu-DOTATOC [37]. Therefore, we can infer that ^{25}Ac-DOTA-rituximab could be a more effective treatment option than ^{131}I-rituximab for NHL patients.

We have performed a clinical trial of RIT for NHL patients using ^{131}I-rituximab for 16 years [8–12]. RIT demonstrated excellent results, but some refractory patients showed resistance to RIT. We expect that it is necessary to treat these refractory patients using more powerful RIT agents. We calculated the probable radiation dose to the tumour and found that ^{225}Ac-DOTA-rituximab revealed a higher radiation dose to the tumour than ^{131}I-rituximab.

Our study has several limitations. First, we analysed only the ^{64}Cu-DOTA-rituximab results in terms of biological experiments. To evaluate the therapeutic effect of ^{225}Ac-DOTA-rituximab more precisely, we need further studies using ^{225}Ac-DOTA-rituximab radiopharmaceutical using an *in vivo* tumour model. Furthermore, clinical trials are warranted to verify the adverse effects and therapeutic effects of ^{225}Ac-DOTA-rituximab. Second, while it has been considered that the lymphoma transgenic mice model will be more clinically relevant than the lymphoma xenograft model, we still preferred to utilise the CD20-positive B-cell lymphoma xenograft model due to the difficulty in evaluating the radiation dosimetry using the small tumour from transgenic mice models. Fortunately, we succeeded in labelling the ^{225}Ac-DOTA-rituximab group (data not shown). In addition, comparison of the therapeutic effect of ^{131}I-rituximab and ^{225}Ac-DOTA-rituximab is ultimately required to confirm the cytotoxicity.

Conclusion

Tumour dosimetry of ^{225}Ac-DOTA-rituximab can be estimated via the Monte Carlo simulation of ^{64}Cu-DOTA-rituximab. ^{225}Ac-DOTA-rituximab can be employed for refractory lymphoma patients as targeted alpha therapy.

Declarations

Funding

This study was supported by a grant from the Korea Institute of Radiological and Medical Sciences (KIRAMS), funded by the Ministry of Science and ICT (MSIT), Republic of Korea (No.50547-2020).

Conflicts of interest

The authors declare that they have no conflicts of interest.

Ethics approval

This study was performed in accordance with the ethical standards of our institutions and with the 1964 Helsinki Declaration and its later amendments or comparable ethical standards.

Availability of data and material

Not applicable.

Author contributions

This study was designed by Chul-Hee Lee, Ilhan Lim, Sang-Keun Woo, Wook Kim, Kwang Il Kim, Kyo Chul Lee, Kanghyon Song, and Sang Moo Lim. Data acquisition and analysis was performed by Chul-Hee Lee, Wook Kim, and Sang-Keun Woo. Chul-Hee Lee and Ilhan Lim wrote the manuscript draft. All authors reviewed and edited this final version of the manuscript.

Consent to participate

Not applicable.

Consent for publication

Not applicable.

References

1. Hagenbeek A. Radioimmunotherapy for NHL: experience of 90Y-ibritumomab tiuxetan in clinical practice. Leuk Lymphoma. 2003;44 Suppl 4:S37-47.

2. Kaminski MS, Estes J, Zasadny KR, Francis IR, Ross CW, Tuck M, Regan D, Fisher S, Gutierrez J, Kroll S, Stagg R, Tidmarsh G, Wahl RL. Radioimmunotherapy with iodine (131)I tositumomab for relapsed or refractory B-cell non-Hodgkin lymphoma: updated results and long-term follow-up of the University of Michigan experience. Blood. 2000;96:1259-66.

3. Kaminski MS, Tuck M, Estes J, Kolstad A, Ross CW, Zasadny K, Regan D, Kison P, Fisher S, Kroll S, Wahl RL. 131I-tositumomab therapy as initial treatment for follicular lymphoma. N Engl J Med. 2005;352:441-9.

4. Bienert M, Reisinger I, Srock S, Humplik BI, Reim C, Kroessin T, Avril N, Pezzutto A, Munz DL. Radioimmunotherapy using 131I-rituximab in patients with advanced stage B-cell non-Hodgkin's lymphoma: initial experience. Eur J Nucl Med Mol Imaging. 2005;32:1225-33.

5. Leahy MF, Seymour JF, Hicks RJ, Turner JH. Multicenter phase II clinical study of iodine-131-rituximab radioimmunotherapy in relapsed or refractory indolent non-Hodgkin's J Clin Oncol. 2006;24:4418-25.

6. Turner Defining pharmacokinetics for individual patient dosimetry in routine radiopeptide and radioimmunotherapy of cancer: Australian experience. Curr Pharm Des. 2009;15:966-82.

7. Kang HJ, Lee SS, Byun BH, Kim KM, Lim I, Choi CW, Suh C, Kim WS, Nam SH, Lee SI, Eom HS, Shin DY, Lim SM. Repeated radioimmunotherapy with 131I-rituximab for patients with low-grade and

aggressive relapsed or refractory B cell non-Hodgkin lymphoma. Cancer Chemother Pharmacol. 2013;71:945-53.

8. Kang GW, Kang HJ, Shin DY, Gu HR, Choi HS, Lim SM. Radioimmunotherapy with (131)i-rituximab in a patient with diffuse large B-cell lymphoma relapsed after treatment with (90)y-ibritumomab tiuxetan. Nucl Med Mol Imaging. 2013;47:281-4.

9. Kang HJ, Lee SS, Kim KM, Choi TH, Cheon GJ, Kim WS, Suh C, Yang SH, Lim SM. Radioimmunotherapy with (131)I-rituximab for patients with relapsed/refractory B-cell non-Hodgkin's lymphoma (NHL). Asia Pac J Clin Oncol. 2011;7:136-45.

10. Lee I, Byun BH, Lim I, Kim BI, Choi CW, Kim KM, Shin DY, Kang HJ, Lim SM. Comparisons of 131I-rituximab treatment responses in patients with aggressive lymphoma and indolent lymphoma. Ann Nucl Med. 2019;33:881-90.

11. Lim I, Park JY, Kang HJ, Hwang JP, Lee SS, Kim KM, Choi TH, Yang SH, Kim BI, Choi CW, Lim SM. Prognostic significance of pretreatment ¹⁸F-FDG PET/CT in patients with relapsed/refractory B-cell non-Hodgkin's lymphoma treated by radioimmunotherapy using ¹³¹I-rituximab. Acta Haematol. 2013;130:74-82.

12. Shin DY, Byun BH, Kim KM, Kang JH, Lim I, Kim BI, Lee SS, Choi CW, Kang HJ, Lim SM. Radioimmunotherapy with (131)I-rituximab as consolidation therapy for patients with diffuse large B-cell lymphoma. Cancer Chemother Pharmacol. 2016;78:825-31.

13. Seidl C. Radioimmunotherapy with α-particle-emitting radionuclides. Immunotherapy. 2014;6:431-58.

14. McDevitt MR, Sgouros G, Finn RD, Humm JL, Jurcic JG, Larson SM, Scheinberg DA. Radioimmunotherapy with alpha-emitting nuclides. Eur J Nucl Med. 1998;25:1341-51.

15. Essler M, Gärtner FC, Neff F, Blechert B, Senekowitsch-Schmidtke R, Bruchertseifer F, Morgenstern A, Seidl C. Therapeutic efficacy and toxicity of 225Ac-labelled vs. 213Bi-labelled tumour-homing peptides in a preclinical mouse model of peritoneal carcinomatosis. Eur J Nucl Med Mol Imaging. 2012;39:602-12.

16. Kratochwil C, Bruchertseifer F, Giesel FL, Weis M, Verburg FA, Mottaghy F, Kopka K, Apostolidis C, Haberkorn U, Morgenstern A. 225Ac-PSMA-617 for PSMA-Targeted α-Radiation Therapy of Metastatic Castration-Resistant Prostate Cancer. J Nucl Med. 2016;57:1941-4.

17. Sgouros G, Roeske JC, McDevitt MR, Palm S, Allen BJ, Fisher DR, Brill AB, Song H, Howell RW, Akabani G, Bolch WE, Brill AB, Fisher DR, Howell RW, Meredith RF, Sgouros G, Wessels BW, Zanzonico PB. MIRD Pamphlet No. 22 (abridged): radiobiology and dosimetry of alpha-particle emitters for targeted radionuclide therapy. J Nucl Med. 2010;51:311-28.

18. Borchardt PE, Yuan RR, Miederer M, McDevitt MR, Scheinberg DA. Targeted actinium-225 in vivo generators for therapy of ovarian cancer. Cancer Res. 2003;63:5084-90.

19. Behling K, Maguire WF, López Puebla JC, Sprinkle SR, Ruggiero A, O'Donoghue J, Gutin PH, Scheinberg DA, McDevitt MR. Vascular Targeted Radioimmunotherapy for the Treatment of Glioblastoma. J Nucl Med. 2016;57:1576-82.

20. Pommé S, Marouli M, Suliman G, Dikmen H, Van Ammel R, Jobbágy V, Dirican A, Stroh H, Paepen J, Bruchertseifer F, Apostolidis C, Morgenstern A. Measurement of the 225Ac half-life. Appl Radiat Isot. 2012;70:2608-14.

21. Reff ME, Carner K, Chambers KS, Chinn PC, Leonard JE, Raab R, Newman RA, Hanna N, Anderson DR. Depletion of B cells in vivo by a chimeric mouse human monoclonal antibody to CD20. Blood. 1994;83:435-45.

22. Kim JY, Park H, Lee JC, Kim KM, Lee KC, Ha HJ, Choi TH, An GI, Cheon GJ. A simple Cu-64 production and its application of Cu-64 ATSM. Appl Radiat Isot. 2009;67:1190-4.

23. Lindmo T, Boven E, Cuttitta F, Fedorko J, Bunn Jr PA. Determination of the immunoreactive function of radiolabeled monoclonal antibodies by linear extrapolation to binding at infinite antigen excess. J Immunol Methods. 1984;72:77-89.

24. Snyder "S" absorbed dose per unit cumulated activity for selected radionuclides and organs. MIRD Pamphlet no. 11. 1975.

25. Natarajan A, Gowrishankar G, Nielsen CH, Wang S, Iagaru A, Goris ML, Gambhir SS. Positron emission tomography of 64Cu-DOTA-Rituximab in a transgenic mouse model expressing human CD20 for clinical translation to image NHL. Mol Imaging Biol. 2012;14:608-16.

26. Woo SK, Jang SJ, Seo MJ, Park JH, Kim BS, Kim EJ, Lee YJ, Lee TS, An GI, Song IH, Seo Y, Kim KI, Kang JH. Development of 64Cu-NOTA-Trastuzumab for HER2 Targeting: A Radiopharmaceutical with Improved Pharmacokinetics for Human Studies. J Nucl Med. 2019;60:26-33.

27. Dahle J, Borrebaek J, Jonasdottir TJ, Hjelmerud AK, Melhus KB, Bruland ØS, Press OW, Larsen RH. Targeted cancer therapy with a novel low-dose rate alpha-emitting radioimmunoconjugate. Blood. 2007;110:2049-56.

28. Dahle J, Borrebaek J, Melhus KB, Bruland OS, Salberg G, Olsen DR, Larsen RH. Initial evaluation of (227)Th-p-benzyl-DOTA-rituximab for low-dose rate alpha-particle radioimmunotherapy. Nucl Med Biol. 2006;33:271-9.

29. Dahle J, Bruland OS, Larsen RH. Relative biologic effects of low-dose-rate alpha-emitting 227Th-rituximab and beta-emitting 90Y-tiuexetan-ibritumomab versus external beam X-radiation. Int J Radiat Oncol Biol Phys. 2008;72:186-92.

30. McLaughlin P, Grillo-López AJ, Link BK, Levy R, Czuczman MS, Williams ME, Heyman MR, Bence-Bruckler I, White CA, Cabanillas F, Jain V, Ho AD, Lister J, Wey K, Shen D, Dallaire BK. Rituximab chimeric anti-CD20 monoclonal antibody therapy for relapsed indolent lymphoma: half of patients respond to a four-dose treatment program. J Clin Oncol. 1998;16:2825-33.

31. Huang SY, Bolch WE, Lee C, Van Brocklin HF, Pampaloni MH, Hawkins RA, Sznewajs A, DuBois SG, Matthay KK, Seo Y. Patient-specific dosimetry using pretherapy [¹²⁴I]m-iodobenzylguanidine ([¹²⁴I]mIBG) dynamic PET/CT imaging before [¹³¹I]mIBG targeted radionuclide therapy for neuroblastoma. Mol Imaging Biol. 2015;17:284-94.

32. Kratochwil C, Schmidt K, Afshar-Oromieh A, Bruchertseifer F, Rathke H, Morgenstern A, Haberkorn U, Giesel FL. Targeted alpha therapy of mCRPC: Dosimetry estimate of 213Bismuth-PSMA-617. Eur J

Nucl Med Mol Imaging. 2018;45:31-7.

33. Wadas TJ, Wong EH, Weisman GR, Anderson CJ. Copper chelation chemistry and its role in copper radiopharmaceuticals. Curr Pharm Des. 2007;13:3-16.

34. McDevitt MR, Ma D, Lai LT, Simon J, Borchardt P, Frank RK, Wu K, Pellegrini V, Curcio MJ, Miederer M, Bander NH, Scheinberg DA. Tumor therapy with targeted atomic nanogenerators. Science. 2001;294:1537-40.

35. Sgouros G, Hobbs RF. Dosimetry for radiopharmaceutical therapy. Semin Nucl Med. 2014;44:172-8.

36. Couturier O, Supiot S, Degraef-Mougin M, Faivre-Chauvet A, Carlier T, Chatal JF, Davodeau F, Cherel M. Cancer radioimmunotherapy with alpha-emitting nuclides. Eur J Nucl Med Mol Imaging. 2005;32:601-14.

37. Azorín-Vega E, Rojas-Calderón E, Ferro-Flores G, Aranda-Lara L, Jiménez-Mancilla N, Nava-Cabrera MA. Assessment of the radiation absorbed dose produced by 177Lu-iPSMA, 225Ac-iPSMA and 223RaCl2 to prostate cancer cell nuclei in a bone microenvironment model. Appl Radiat Isot. 2019;146:66-71.

Tables

Table 1 Normal organ absorbed dose of ^{64}Cu-DOTA-Rituximab calculated with OLINDA male adult phantom

	OLINDA	
	^{64}Cu-DOTA-Rituximab Absorbed dose (mGy/MBq)	
	Mean	SD
Adrenals	7.37E-03	4.69E-03
Brain	4.20E-03	3.13E-03
Breasts	1.72E-03	1.16E-03
Gallbladder Wall	1.07E-02	5.43E-03
LLI Wall	1.96E-03	6.35E-04
Small Intestine	4.23E-02	2.57E-02
Stomach Wall	1.73E-02	7.37E-03
ULI Wall	4.40E-02	2.60E-02
Heart Wall	2.33E-02	1.44E-02
Kidneys	1.63E-01	1.01E-01
Liver	9.09E-02	6.74E-02
Lungs	3.46E-02	2.67E-02
Muscle	2.13E-03	1.11E-03
Ovaries	3.35E-03	1.16E-03
Pancreas	7.09E-03	3.68E-03
Red Marrow	2.53E-03	1.00E-03
Osteogenic Cells	1.52E-03	7.69E-04
Skin	9.22E-04	4.85E-04
Spleen	6.61E-02	4.11E-02
Testes	2.42E-04	4.42E-05
Thymus	2.25E-03	1.52E-03
Thyroid	7.68E-02	7.10E-02
Urinary Bladder Wall	9.67E-04	1.14E-04
Uterus	2.63E-03	7.96E-04
Total Body	6.15E-03	3.24E-03

Effective dose (mSv/MBq)	3.20E-02	1.19E-02

Figures
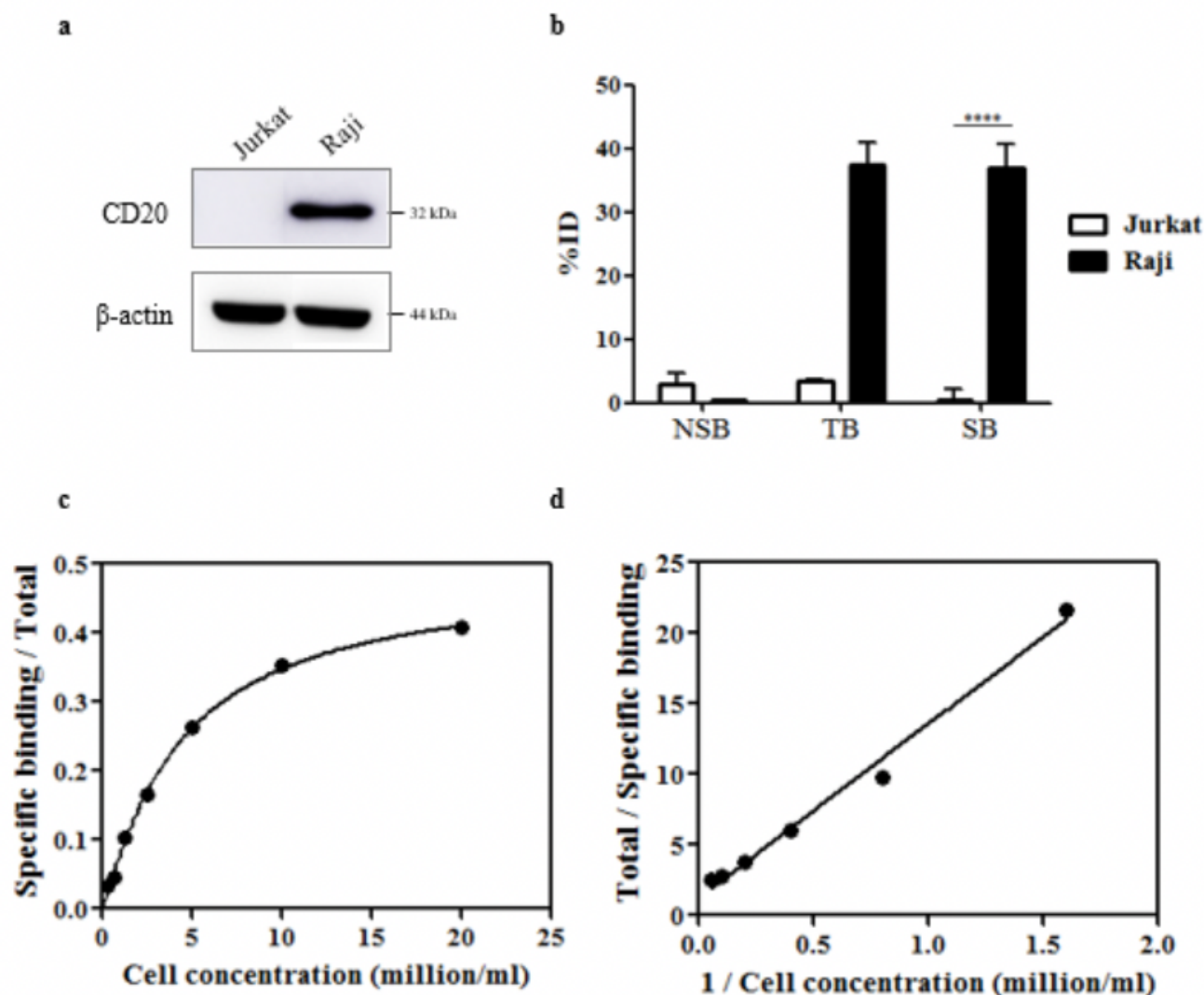
Figure 1

CD20 expression and 64Cu-DOTA-ritxuaimb binding a Western blot analysis of CD20. β-actin was used as an internal control. CD20 expression was observed in Raji cells. b Cell binding assay of 64Cu-DOTA-rituximab Specific binding (SB) of Raji cells was 90-fold higher than that of Jurkat cells (p<0.0001). c and d Immunoreactivity assay (Lindmo assay) using Raji cells. d was analysed using GraphPad software from c. Immunoreactivity was 76%
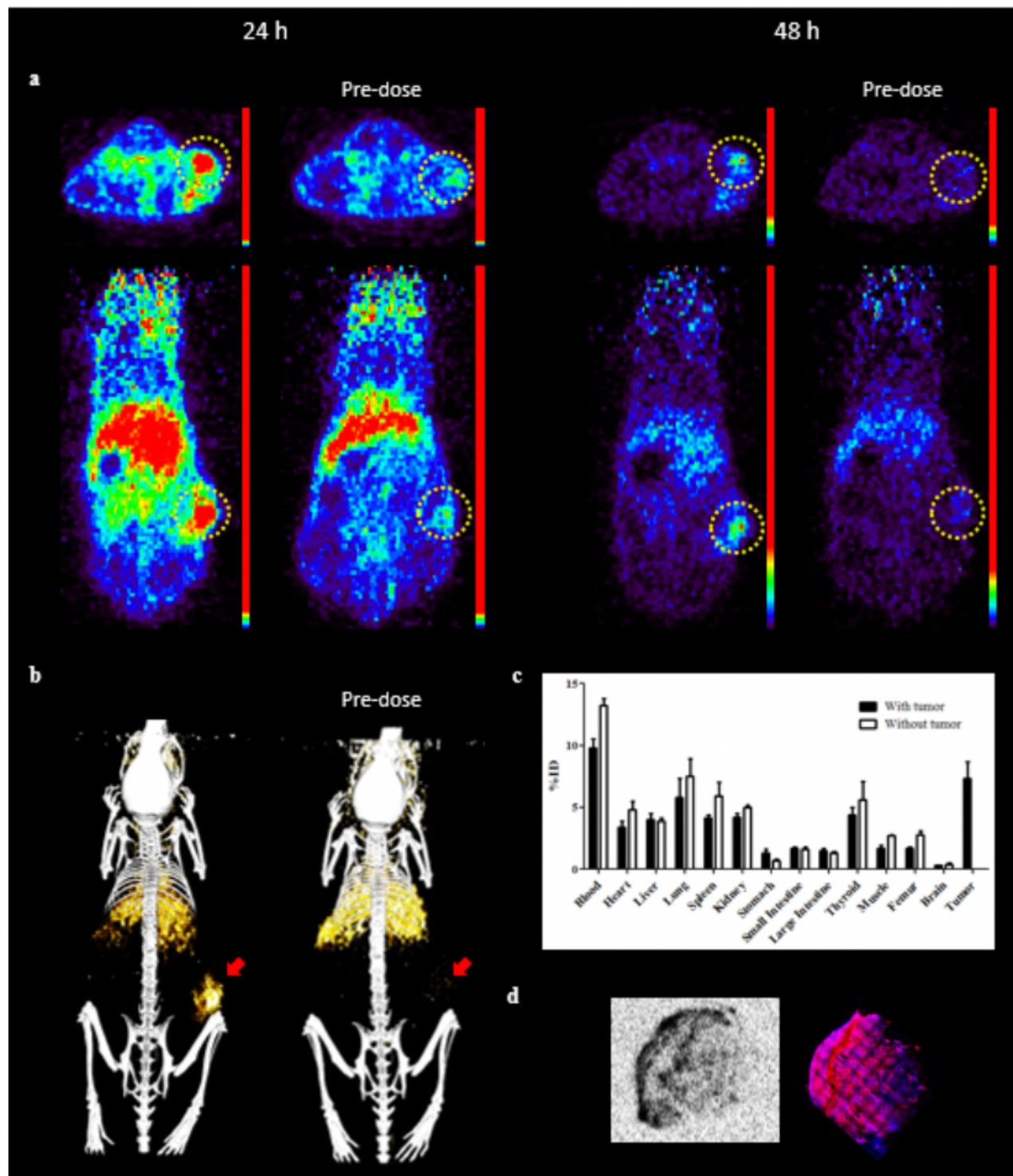
Figure 2

In vivo lymphoma models and 64Cu-DOTA-rituximab PET/CT imaging a 64Cu-DOTA-rituximab PET imaging at 24 and 48 h with (n=2) and without (n=3) blocking by cold-rituximab. b Representative PET/CT imaging at 48 h using 3D visualisation software. Tumour-targeted imaging was observed. c Biodistribution study with (n=3) and without (n=4) lymphoma at 48 h. Accumulation in the tumour was

the second highest. d Autoradiography (64Cu-DOTA-rituximab) and immunostaining (CD20) images showed a correlation
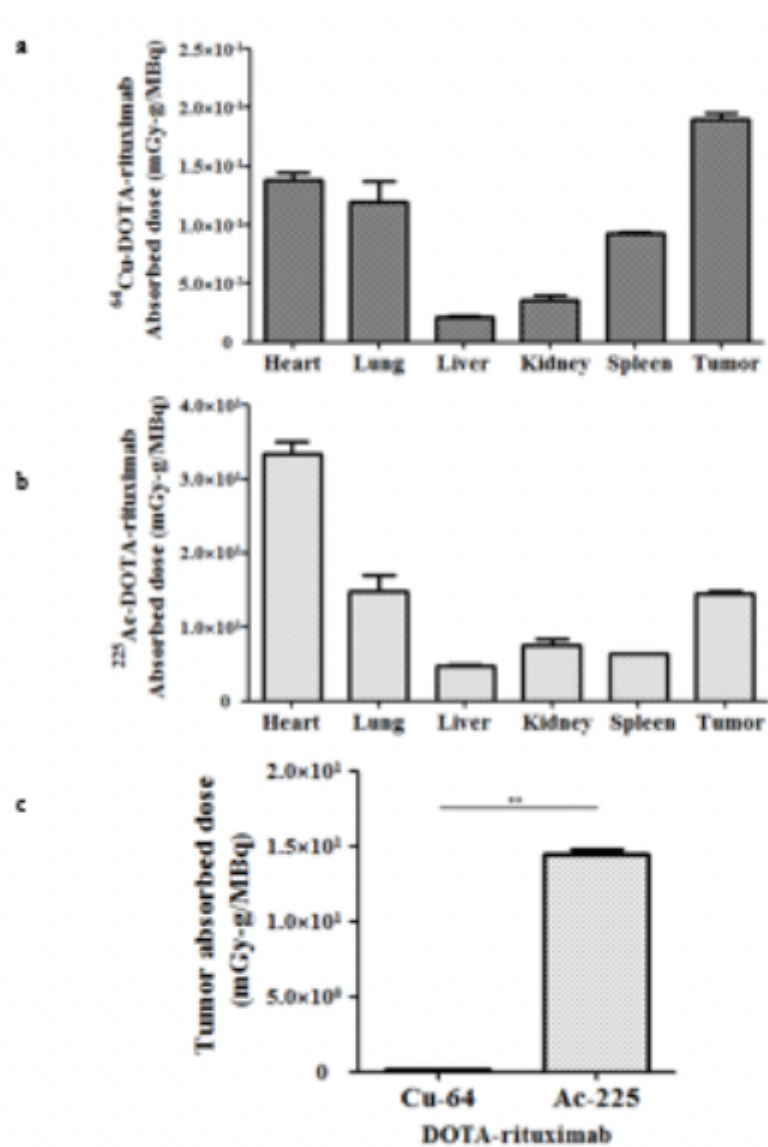
Figure 3

Absorbed dose estimation of 64Cu- and 225Ac-DOTA-rituximab using Monte Carlo simulation. a Absorbed dose of 64Cu-DOTA-rituximab in mouse tumour model. b Absorbed dose of 225Ac-DOTA-rituximab in mouse tumour model. c Relative absorbed dose in tumours of Cu-64 or Ac-225 (P < 0.01). Data were obtained from a and b